



Catalytic surface promotion of highly active $\text{La}_{0.85}\text{Sr}_{0.15}\text{Cr}_{0.8}\text{Ni}_{0.2}\text{O}_{3-\delta}$ anodes for $\text{La}_{5.6}\text{WO}_{11.4-\delta}$ based proton conducting fuel cells

C. Solís^a, M. Balaguer^a, F. Bozza^b, N. Bonanos^b, J.M. Serra^{a,*}

^a Instituto de Tecnología Química (Universidad Politécnica de Valencia - Consejo Superior de Investigaciones Científicas), Avenida de los Naranjos s/n, 46022 Valencia, Spain

^b Department of Energy Conversion and Storage Technical University of Denmark-DTU, P.O. Box 49, 4000 Roskilde, Denmark



ARTICLE INFO

Article history:

Received 5 July 2013

Received in revised form 21 August 2013

Accepted 26 August 2013

Available online 1 September 2013

Keywords:

Anode

Proton conducting fuel cell

Chromite

Lanthanum tungstate

Catalyst

ABSTRACT

$\text{La}_{0.85}\text{Sr}_{0.15}\text{CrO}_{3-\delta}$ (LSC), $\text{La}_{0.85}\text{Sr}_{0.15}\text{Cr}_{0.8}\text{Ni}_{0.2}\text{O}_{3-\delta}$ (LSCN) and LSCN infiltrated with Ni nanoparticles were tested as anodes for symmetrical cells based on $\text{La}_{5.6}\text{WO}_{11.4-\delta}$ (LWO) protonic electrolyte. These chromite-based electrode materials are compatible with LWO material, in contrast to the widely used NiO. Under typical anode reducing conditions, Ni is segregated from the LSCN lattice on the grain surface as metallic Ni nanoparticles, which are proved to be compatible with LWO in reducing conditions. These Ni nanoparticles become the catalytic active sites for the H_2 oxidation reaction in proton conducting anodes and the electrode performance is substantially improved regarding to pure LSC. Ni nanoparticle infiltration further improves the catalytic promotion of the anode, reducing the polarization resistance (R_p) previously limited by low frequency surface related processes. Indeed, the R_p values achieved for LSCN infiltrated with Ni, e.g. $0.47 \Omega \text{ cm}^2$ at 700°C , suggest the practical application of this kind of anodes in proton conducting solid oxide fuel cells (PC-SOFC).

© 2013 Elsevier B.V. All rights reserved.

1. Introduction

Proton conducting solid oxide fuel cells (PC-SOFCs) can be operated in the intermediate temperature range (500 – 800°C) and avoid the fuel dilution, since water is formed in the air electrode, in contrast with conventional SOFC. [1] $\text{La}_{6-x}\text{WO}_y$ (LWO) with $0.4 < x < 0.7$ is a mixed ionic (protonic)-electronic conducting material with predominant protonic transport at temperatures up to 800°C and under fuel cell operating conditions. [2–9] The oxygen stoichiometry (y) depends on the La/W ratio and the concrete W oxidation state. Additionally, it exhibits high stability in CO_2 containing atmospheres, being a promising candidate as electrolyte for PC-SOFC electrolyte. [10]

The use of the LWO as electrolyte material demands new compatible anodes, as the most common anode material, NiO, readily reacts with LWO during the sintering step, destroying the LWO phase. [11] Previous studies on Ni doped $\text{La}_{0.85}\text{Sr}_{0.15}\text{CrO}_{3-\delta}$ anodes show good results in both conventional SOFCs and PC-SOFCs, since they combine sufficient electronic, oxygen-ion and protonic conductivity under anode operation conditions, together with catalytic activity due to the incorporation of nickel. [11–14] After the reduction, the material splits the structural Ni, which acts as catalyst

for H_2 bond breaking and steam reforming of natural gas. [15,16] Its compatibility with LWO (both chromite phase and metallic Ni particles) makes it a promising candidate as anode for LWO based PC-SOFC. [11,14] Indeed, the recently proved good performance of $\text{La}_{0.75}\text{Sr}_{0.15}\text{Ce}_{0.1}\text{CrO}_{3-\delta}$ (LSCCe) anode on LWO electrolyte and the great improvement achieved by Ni infiltration strategies constitute the basis for the present study. [17]

In this work $\text{La}_{0.85}\text{Sr}_{0.15}\text{CrO}_{3-\delta}$ (LSC), $\text{La}_{0.85}\text{Sr}_{0.15}\text{Cr}_{0.8}\text{Ni}_{0.2}\text{O}_{3-\delta}$ (LSCN) and LSCN infiltrated with Ni nanoparticles are tested as anodes for LWO based PC-SOFCs aiming (1) to compare results of the new Ni doped LSC material with previously studied LSC based anodes and (2) to analyze the effect of the surface catalytic promotion due to the Ni infiltration.

2. Experimental

The citrate reaction route was used for preparing $\text{La}_{0.85}\text{Sr}_{0.15}\text{CrO}_{3-\delta}$ (LSC) and $\text{La}_{0.85}\text{Sr}_{0.15}\text{Cr}_{0.8}\text{Ni}_{0.2}\text{O}_{3-\delta}$ (LSCN) powders, as described elsewhere, with a final sintering temperature of 800 and 900°C respectively. [15,18] $\text{La}_{5.6}\text{WO}_{11.4-\delta}$ (LWO) electrolyte powder was commercially provided by Cerpotech.

The phase composition of the different materials was characterized by X-ray diffraction (XRD) by a PANalytical Cubix diffractometer, using $\text{CuK}\alpha_{1,2}$ radiation and a X'Celerator detector in Bragg–Brentano geometry. XRD patterns were recorded in the

* Corresponding author. Tel.: +34 9638 79448; fax: +34 9638 77809.

E-mail address: jmserra@itq.upv.es (J.M. Serra).

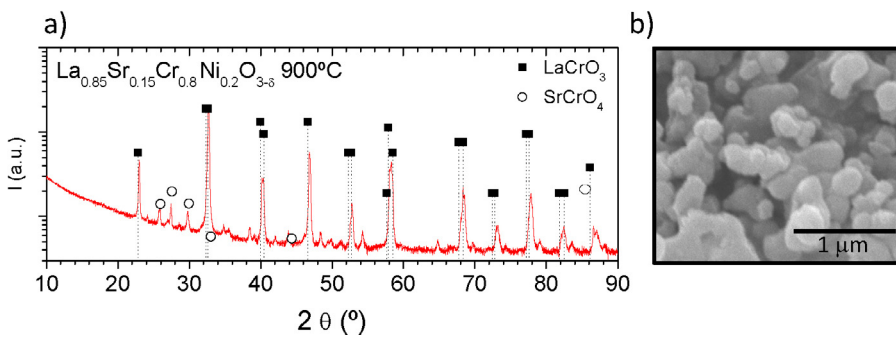


Fig. 1. XRD pattern (a) and SEM image (b) of LSCN powder sintered at 900 °C.

2θ range from 10° to 90° and analyzed using X'Pert Highscore Plus software.

Dense ~1 mm-thick LWO disks were obtained by uniaxially pressing the ball-milled LWO powder at ~120 MPa and final firing at 1500 °C for 5 h. Porous ~15 μm electrodes were obtained by screen-printing chromite inks on both sides of LWO electrolyte disks. Firing temperature of the screen-printed anodes was 1150 °C for 2 h.

The final size of the symmetrical cells was 15.5 mm in diameter, whereas anodes were ~9 mm in diameter. A gold mesh was screen-printed on the surface of both anodes for helping the electronic contact with the electrodes.

The Ni infiltration procedure was made by using 5 M water solution of Ni Nitrate (LSCN + 5Ni). The solutions were dropped on the surface of the electrodes and allowed to penetrate into the electrodes pores for 30 min. Afterwards it was calcined at 300 °C to decompose the nitrates. The process was repeated 4 times.

LSCN/LWO/LSCN symmetrical cells were tested by electrochemical impedance spectroscopy (EIS) in two-point configuration with platinum current collector meshes. Input signal was 0 V DC–20 mV AC in the 0.01–3 × 10⁵ Hz frequency range. This signal was generated by a Solartron 1470E and a 1455A FRA module equipment. EIS measurements were performed in the 600–800 °C range, under moistened atmospheres (2.5% vol. H₂O) at different pH₂ (1, 0.5 and 0.05 atm) and in wet 5% D₂ (2.5% vol. D₂O). In all the cases, the total flow remained constant (100 mL min⁻¹). All the impedance spectra have been corrected by removing the contribution of the LWO electrolyte, i.e., the high frequency real axis cut-off in the Nyquist diagrams.

The microstructure was investigated using scanning electron microscopy (SEM) (Zeiss Ultra 55), and elemental analysis was carried out with energy-dispersive X-ray spectroscopy (EDS) (INCA, Oxford).

3. Results and discussion

The structure of the LSCN powder sintered at 900 °C can be observed from XRD pattern plotted in Fig. 1a. The main diffraction peaks can be assigned to the orthorhombic LaCrO_{3-δ} perovskite phase, although some traces of SrCrO₄ spinel phase can be also observed. [19] These traces of SrCrO₄ have also been previously observed at this low sintering temperature but it has also been proved that they disappear upon exposure to reducing conditions. [15] SEM image in Fig. 1b shows the microstructure of this powder, which presents homogenous grain size distribution.

Different symmetrical cells were prepared on LWO electrolyte by using LSC and LSCN inks, and also by the Ni infiltration of the LSCN electrode (LSCN + 5Ni). XRD patterns of the different symmetrical cells, LSC, LSCN and LSCN + 5Ni, are represented in Fig. 2 (intensity in log scale) after the impedance measurements at high

temperature (up to 800 °C) and reducing conditions. The diffraction peaks of the LSC electrode can be assigned to (1) the chromite perovskite phase, (2) the LWO electrolyte fluorite phase and (3) the metallic Au, screen printed on the surface of the anode as current collector in the symmetrical cell testing. As expected after the high temperature and the reducing conditions, no traces of SrCrO₄ were observed. [15] The reducing conditions at high temperature produced the segregation of metallic Ni in the doped anode (LSCN symmetrical cell), as inferred from the diffraction peaks assigned to Ni metal in agreement with previous works. [11,15] This Ni segregation gives rise to the formation of cationic defects. [20] The intensity of the Ni diffraction peaks is increased in the case of LSCN + 5Ni symmetrical cell, as corresponds to the much higher amount, i.e., grain surface coverage, of Ni of this sample due to the Ni infiltration. [21]

The Ni nanoparticles segregation out from the LSCN perovskite structure under anode operation conditions (high temperature and reducing atmospheres) is represented in the scheme of Fig. 3a. However, from its real SEM image, shown in Fig. 3b, it is not easy to distinguish the presence of these nanoparticles, due to the very small amount of Ni. For this reason, in previous reported works, TEM was used for the characterization of this particles segregation (see Fig. S1 in supporting material) [11,15]. The scheme of the LSCN electrode when it is infiltrated by using 5 M water solution of Ni nitrate (LSCN + 5Ni) is shown in Fig. 3c and corresponding SEM images of the cross section anodes after impedance measurements are depicted in Fig. 3d and e at two different magnifications. LSCN + 5Ni SEM images show the high density of Ni nanoparticles homogeneously covering the LSCN grains along the whole thickness of the electrode, preserving the porous backbone structure, as Ni was added after the electrode sintering. The average Ni particle size (10–20 nm) is similar to that of the Ni powder reduced from precursor nitrates shown elsewhere. [17]

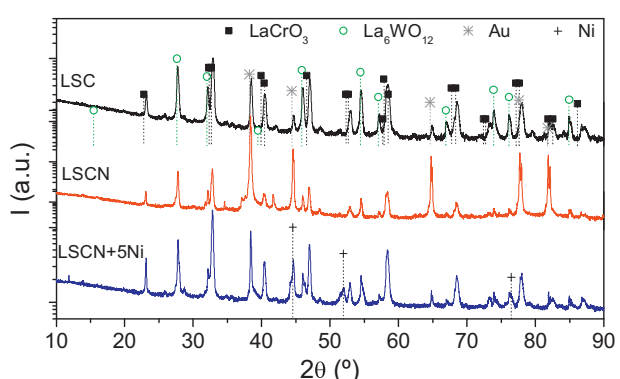


Fig. 2. XRD patterns of LSC, LSCN and LSCN + 5Ni symmetrical cells, after impedance measurements.

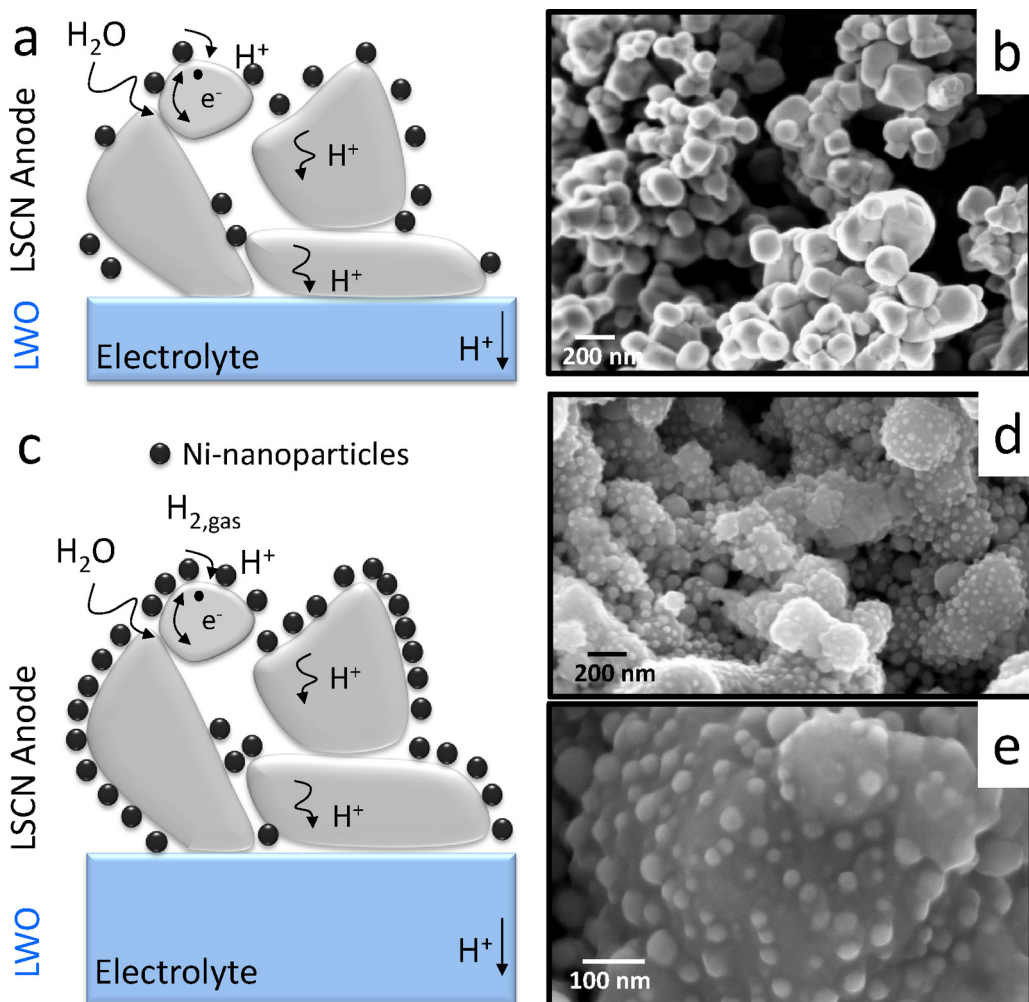


Fig. 3. Schematic diagram of the LSCN anode (a) and its corresponding SEM image (b) and scheme of the LSCN + 5Ni anode (c) and its real SEM images (d and e).

Supplementary material related to this article can be found, in the online version, at <http://dx.doi.org/10.1016/j.apcatb.2013.08.044>.

Electrochemical properties of the three different tested anodes, LSC, LSCN and LSCN + 5Ni, can be analyzed from the polarization resistance (R_p) values as a function of the temperature, plotted in Fig. 4. At 700 °C in hydrogen LSC anode shows a R_p of 347 Ω cm². The segregation of Ni nanoparticles on LSCN electrode decreases R_p two orders of magnitude, up to 3.54 Ω cm². This great improvement points out the importance of the Ni nanoparticles catalyzing the H₂ oxidation reaction. When the amount of catalyst is increased, by further Ni infiltration of LSCN anode (LSCN + 5Ni), electrochemical properties are strongly improved, reaching a R_p of 0.47 Ω cm² at 700 °C.

In order to corroborate the catalytic improvement of the anodes with Ni nanoparticles segregated from the structure on one hand and obtained by Ni infiltration on the other, EIS spectra were analyzed for the three different symmetrical cells.

Fig. 5 shows EIS spectra at 700 °C of LSC anode (a and b, Nyquist and Bode plots respectively) and of both LSCN and LSCN + 5Ni (c and d, Nyquist and Bode plots) after subtracting the electrolyte contribution. These spectra (corresponding to LSC and LSCN anodes) show two main contributions, two different arcs, at two different frequency ranges. LSC anode is limited by low frequency (LF) associated processes, although it also shows an important contribution of the high frequency (HF) associated

processes. When the material is doped with Ni (LSCN electrode), and thus active Ni nanoparticles are segregated to the surface of the material under operating conditions, this LF contribution is drastically decreased (almost two orders of magnitude), although

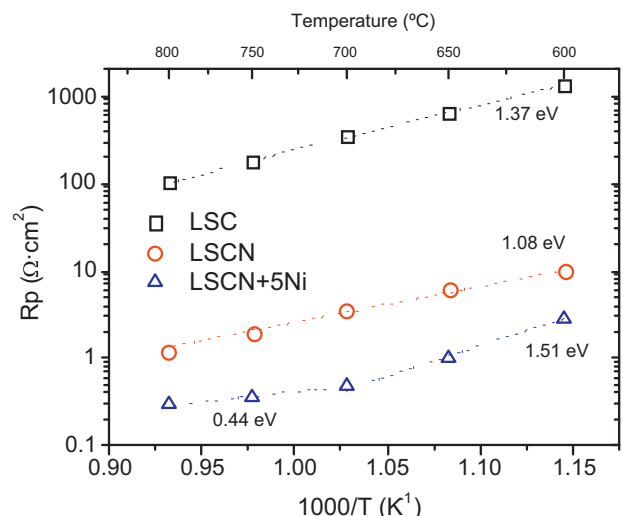


Fig. 4. R_p as a function of inverse temperature of LSC, LSCN and LSCN + 5Ni symmetrical cells.

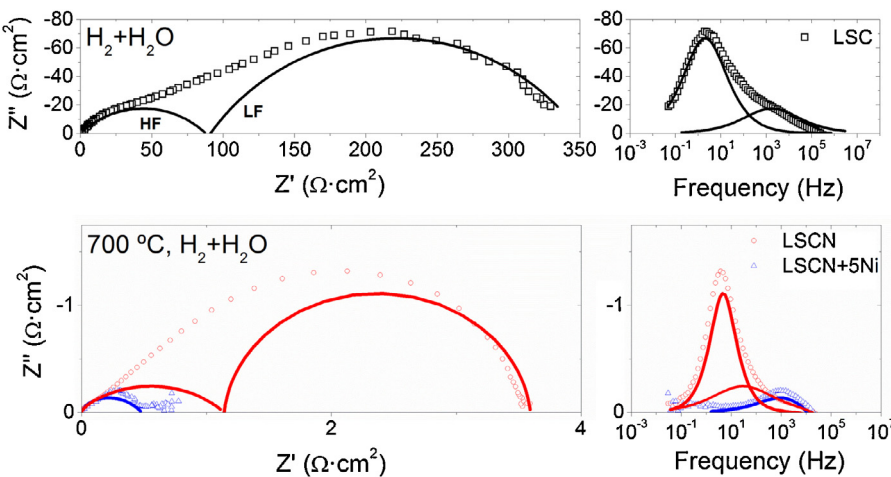


Fig. 5. Impedance spectra recorded at 700 °C in wet hydrogen (2.5% H₂O in pure H₂) of LSC (a) Nyquist and (b) Bode plots of LSCN and LSCN + 5Ni (c) Nyquist and (d) Bode plots. Solid lines represent the fittings to HF and LF contributions.

it is still limiting the anode performance. LSCN anode also shows another contribution at higher frequencies. With the addition of more active Ni nanoparticles by infiltration (LSCN + 5Ni), the LF contribution disappears and a high frequency (HF) associated processes become the limiting contribution. Thus LSCN + 5Ni anode only shows one main contribution, although at low frequencies there is a small noise ascribed to the contacts, only visible at high temperatures.

These different HF and LF contributions can be analyzed in terms of two (or one) depressed arcs by fitting EIS spectra to a double R||CPE circuit (or single in the case of LSCN + 5Ni anode). The depressed arcs need the use of these CPEs (Constant Phase Elements) instead of a capacitor as corresponds to the porous structure of the electrode. The impedance of a CPE can be expressed as:

$$Z_{\text{CPE}} = A^{-1}(j\omega)^{-n} \quad (1)$$

where A is a constant that is independent of frequency, ω is the angular frequency and $j = \sqrt{-1}$. [22] The equivalent capacitance of the CPEs can be calculated according to: [23]

$$C_{\text{CPE}} = R^{(1-n)/n} A^{1/n} \quad (2)$$

The modelled resistances and capacitances (calculated from CPEs) are depicted in Fig. 6a and b. Solid lines represent the fittings to HF and LF contributions and the characteristic frequencies are written in the graph. Solid lines represent the fittings to HF and LF contributions.

LSC anode shows limiting LF (2–25 Hz) contributions with associated capacitances of 10^{-3} F cm⁻², which can be assigned to surface processes. These surface processes are typically H₂ adsorption and dissociation into singular species (H⁺ or H). Note that gas diffusion can be dismissed as it is fairly insensitive to temperature and the activation energy (E_a) of these LF processes is 1.04 eV. [21] LSC also presents very high resistance in the HF (1–10 kHz) range, with capacitances ranging from 10^{-5} to 10^{-4} F cm⁻², that can be associated with LSC transport properties.

With the Ni dopant, and the consequent Ni nanoparticles formation on the surface of the chromite, LSCN shows LF (10–100 Hz) and medium frequencies (MF, range 0.1–0.5 kHz) contributions. By taking into account their associated capacitances, of 10^{-2} F cm⁻² for LF and 10^{-3} to 10^{-2} F cm⁻² for MF processes, both can be assigned to surface related processes. In particular, the MF is associated to surface exchange coupled with bulk ionic transport in mixed conducting electrodes. [17,22,24] On the other hand, LF resistance decreases more than one order of magnitude compared to that of LSC and its characteristic frequencies shift to higher values. This

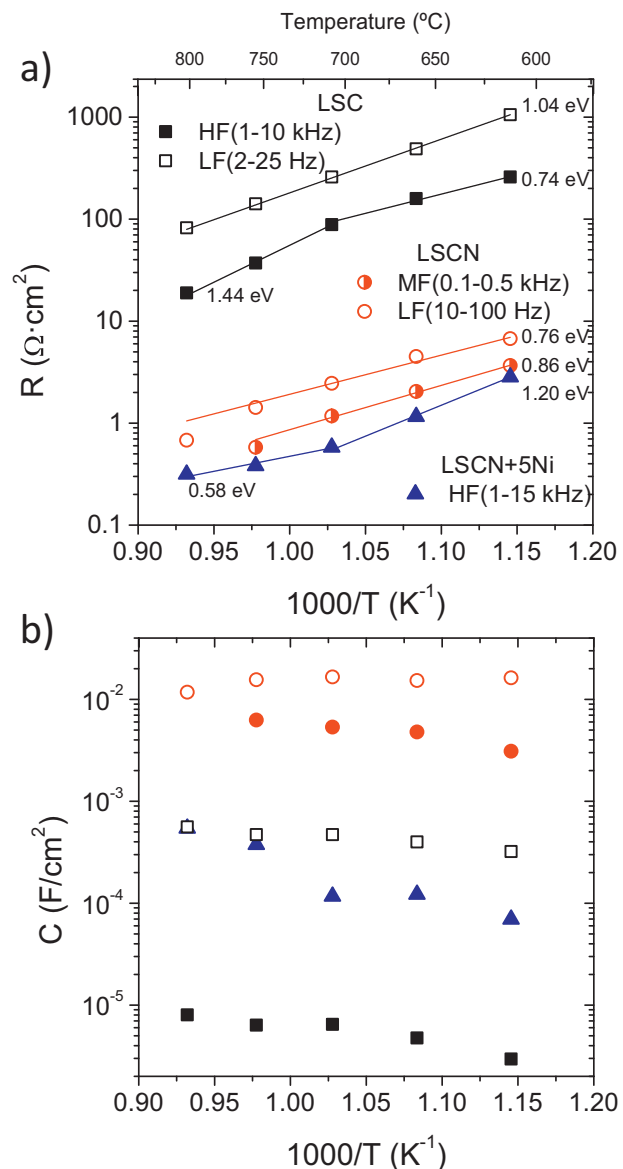


Fig. 6. Temperature dependency of modelled resistances (a) and capacitances (b) of LSC, LSCN and LSCN + 5Ni samples.

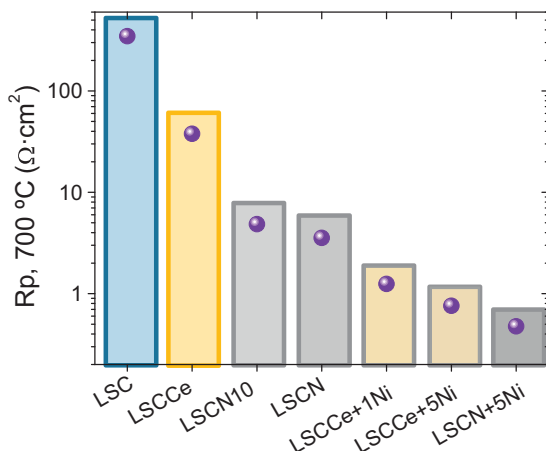


Fig. 7. R_p at 700 °C of different chromite based anodes: $\text{La}_{0.85}\text{Sr}_{0.15}\text{CrO}_{3-\delta}$ (LSC), $\text{La}_{0.75}\text{Sr}_{0.15}\text{Ce}_{0.1}\text{CrO}_{3-\delta}$ (LSCCe)[17], $\text{La}_{0.85}\text{Sr}_{0.15}\text{Cr}_{0.9}\text{Ni}_{0.1}\text{O}_{3-\delta}$ (LSCN10)[11], $\text{La}_{0.85}\text{Sr}_{0.15}\text{Cr}_{0.8}\text{Ni}_{0.2}\text{O}_{3-\delta}$ (LSCN), LSCCe+1Ni[17], LSCCe+5Ni [17] and LSCN+5Ni.

LF resistance drop can only be attributed to the beneficial effect of the active Ni nanoparticles, well-known catalysts of hydrogen dissociation. The high catalytic activity of these Ni nanoparticles is demonstrated with the disappearance of the LF contributions in the LSCN + 5Ni anode, with higher density of active Ni nanoparticles on the surface (as shown in Fig. 3).

Thus LSCN + 5Ni anode only shows high frequency HF (1–15 kHz) contributions with associated capacitances of 10^{-3} to $10^{-4} \text{ F cm}^{-2}$. These HF associated processes could be ascribed to either the transport properties of the LSCN material or to the charge transfer reaction at the electrode/electrolyte interface: [25] (i) the charge transfer between Ni nanoparticles and the oxide and (ii) the diffusion of charged species to the three phase boundary. [26] In fact the observed change in the E_a of the HF resistance, produced at around at 700 °C, can be directly related to the change in the E_a of the transport properties of this material, and ascribed to the variation of the predominant charge carriers with temperature. [11]

In conclusion, the pronounced impedance improvement suggests that Ni infiltration is a proper method to promote the catalytic activity of LSC-based electrodes towards H₂ oxidation, since high Ni dispersion, i.e. active surface area, on the LSC grains is achieved, while keeping the small particle size during operation.

As a summary, a complete comparison between different chromite-based anodes on LWO electrolytes can be seen in Fig. 7, where R_p at 700 °C is plotted for LSC, $\text{La}_{0.75}\text{Sr}_{0.15}\text{Ce}_{0.1}\text{CrO}_{3-\delta}$ (LSCCe) [17], $\text{La}_{0.85}\text{Sr}_{0.15}\text{Cr}_{0.9}\text{Ni}_{0.1}\text{O}_{3-\delta}$ (LSCN10) [11], $\text{La}_{0.85}\text{Sr}_{0.15}\text{Cr}_{0.8}\text{Ni}_{0.2}\text{O}_{3-\delta}$ (LSCN, this study), LSCCe + 1Ni [17], LSCCe + 5Ni [17] and LSCN + 5N (this study). The graph depicts the gradual decrease of the R_p from the $347 \Omega \cdot \text{cm}^2$ obtained for LSC to 4.85 and $3.55 \Omega \cdot \text{cm}^2$ when the LSC material is firstly substituted by 10 and 20% Ni, respectively and $37.81 \Omega \cdot \text{cm}^2$ obtained for 10% Ce doped LSC. This anode improvement is increased with the further Ni infiltration on both LSCCe and LSCN anodes, being LSCN + 5Ni anode the best electrode ($R_p = 0.47 \Omega \cdot \text{cm}^2$) with slightly better performance than LSCCe + 5Ni ($R_p = 0.76 \Omega \cdot \text{cm}^2$).

4. Conclusions

Catalytic surface engineering of LWO compatible chromite-based materials enabled the improvement of PC-SOFCs anodes. $\text{La}_{0.85}\text{Sr}_{0.15}\text{CrO}_{3-\delta}$ (LSC), $\text{La}_{0.85}\text{Sr}_{0.15}\text{Cr}_{0.8}\text{Ni}_{0.2}\text{O}_{3-\delta}$ (LSCN) and LSCN infiltrated with Ni nanoparticles (LSCN + 5Ni) anodes are compared in symmetrical cell configuration. Under typical anode reducing conditions, structural Ni is segregated on the surface. These Ni nanoparticles are catalytically active for the H₂ oxidation reaction improving the anode performance regarding to pure LSC. Ni infiltration leads to additional catalytic promotion of the anode, further reducing the R_p previously limited by low frequency surface related processes. Indeed, $R_p = 0.47 \Omega \cdot \text{cm}^2$ obtained for LSCN infiltrated with Ni (LSCN + 5Ni) make this anode suitable for PC-SOFC anode, fulfilling the current requirements for practical operation.

Acknowledgements

Funding from European Union (FP7 Project EFFIPRO – Grant Agreement 227560), the Spanish Government (ENE2011-24761, SEV-2012-0267 and CSIC Intramural 200880I093 grants) is kindly acknowledged. The authors thank M. Fabuel for sample preparation.

References

- [1] H. Iwahara, Solid State Ionics 77 (1995) 289–298.
- [2] R. Haugsrud, C. Kjøseth, Journal of Physics and Chemistry of Solids 69 (2008) 1758–1765.
- [3] C. Solís, S. Escalastico, R. Haugsrud, J.M. Serra, Journal of Physical Chemistry C 115 (2011) 11124–11131.
- [4] A. Magraso, J.M. Polfus, C. Frontera, J. Canales-Vazquez, L.-E. Kalland, C.H. Hervoches, S. Erdal, R. Hancke, M.S. Islam, T. Norby, R. Haugsrud, Journal of Materials Chemistry 22 (2012) 1762–1764.
- [5] S. Escalastico, C. Solís, J.M. Serra, International Journal of Hydrogen Energy 36 (2011) 11946–11954.
- [6] S. Escalastico, V.B. Vert, J.M. Serra, Chemistry of Materials 21 (2009) 3079–3089.
- [7] C. Solís, L. Navarrete, S. Roitsch, J.M. Serra, Journal of Materials Chemistry 22 (2012) 16051–16059.
- [8] C. Solís, L. Navarrete, J.M. Serra, Journal of Power Sources 240 (2013) 691–697.
- [9] T. Scherb, S.A.J. Kimber, C. Stephan, P.F. Henry, G. Schumacher, J. Just, S. Escalastico, J.M. Serra, J. Seeger, A.H. Hill, J. Banhart, arXiv:1305.3385.
- [10] S. Escalástico, C. Solís, T. Scherb, G. Schumacher, J.M. Serra, Journal of Membrane Science 444 (2013) 276–284.
- [11] C. Solís, V.B. Vert, M. Balaguer, S. Escalastico, S. Roitsch, J.M. Serra, ChemSusChem 5 (2012) 2155–2158.
- [12] J. Steir, Journal of Power Sources 118 (2003) 276–285.
- [13] A.L. Sauvet, J.T.S. Irvine, Solid State Ionics 167 (2004) 1–8.
- [14] S. Li, S. Wang, Y. Wang, H. Nie, T.L. Wen, Fuel Cells 6 (2006) 451–454.
- [15] V.B. Vert, F.V. Melo, L. Navarrete, J.M. Serra, Applied Catalysis B: Environmental 115–116 (2012) 346–356.
- [16] M.V. Twigg Catalyst Handbook, 2 ed., Manson Publishing, London, 1996.
- [17] M. Balaguer, C. Solís, F. Bozza, N. Bonanos, J.M. Serra, Journal of Materials Chemistry A 1 (2013) 3004–3007.
- [18] J.M. Serra, V.B. Vert, M. Betz, V.A.C. Haanappel, W.A. Meulenberg, F. Tietz, Journal of the Electrochemical Society 155 (2008) B207–B214.
- [19] B.I. Lee, R.K. Gupta, C.M. Whang, Materials Research Bulletin 43 (2008) 207–221.
- [20] M. Oishi, K. Yashiro, J.O. Hong, Y. Nigara, T. Kawada, J. Mizusaki, Solid State Ionics 178 (2007) 307–312.
- [21] S. Primdahl, M. Mogensen, Solid State Ionics 152 (2002) 597–608.
- [22] E. Barsoukov, J.R.I. Macdonald, Impedance Spectroscopy Theory, Experiment, and Applications, John Wiley & Sons, 2005.
- [23] C.H. Hsu, F. Mansfeld, Corrosion 57 (2001) 747–748.
- [24] S.B. Adler, J.A. Lane, B.C.H. Steele, Journal of The Electrochemical Society 143 (1996) 3554–3564.
- [25] S.P. Jiang, S.P.S. Badwal, Solid State Ionics 123 (1999) 209–224.
- [26] J.M. Serra, V.B. Vert, Journal of The Electrochemical Society 157 (2010) B1349–B1357.